Inorganic Chemistry

Article

pubs.acs.org/IC

Re and Br X-ray Absorption Near-Edge Structure Study of the Ground and Excited States of [ReBr(CO)$_3$(bpy)] Interpreted by DFT and TD-DFT Calculations

Stanislav Záliš,*[,†] Chris J. Milne,*[,‡,∥] Amal El Nahhas,[‡,⊥] Ana María Blanco-Rodríguez,[§] Renske M. van der Veen,[‡,#] and Antonín Vlček, Jr.*[,†,§]

[†]J. Heyrovský Institute of Physical Chemistry, Academy of Sciences of the Czech Republic, Dolejškova 3, CZ-182 23 Prague, Czech Republic

[‡]Laboratoire de Spectroscopie Ultrarapide, Ecole Polytechnique Fédérale de Lausanne, ISIC-FSB, Station 6, CH-1015 Lausanne, Switzerland

[§]School of Biological and Chemical Sciences, Queen Mary University of London, Mile End Road, London E1 4NS, United Kingdom

Supporting Information

ABSTRACT: X-ray absorption spectra of *fac*-[ReBr(CO)$_3$(bpy)] near the Re L$_3$- and Br K-edges were measured in a steady-state mode as well as time-resolved at 630 ps after 355 nm laser pulse excitation. Relativistic spin−orbit time-dependent density functional theory (TD-DFT) calculations account well for the shape of the near-edge absorption (the "white line") of the ground-state Re spectrum, assigning the lowest-lying transitions as core-to-ligand metal-to-ligand charge transfer from Re 2p$_{3/2}$ into predominantly π^*(bpy) molecular orbitals (MOs) containing small 5d contributions, followed in energy by transitions into π^* Re(CO)$_3$ and delocalized σ^*/π^* MOs. Transitions gain their intensities from Re 5d and 6s participation in the target orbitals. The 5d character is distributed over many unoccupied MOs; the 5d contribution to any single empty MO does not exceed 29%. The Br K-edge spectrum is dominated by the ionization edge and multiple scattering features, the pre-edge electronic transitions being very weak. Time-resolved spectra measured upon formation of the lowest electronic excited state show changes characteristic of simultaneous Re and Br electronic depopulation: shifts of the Re and Br edges and the Re white line to higher energies and emergence of new intense pre-edge features that are attributed by TD-DFT to transitions from Re 2p$_{3/2}$ and Br 1s orbitals into a vacancy in the HOMO-1 created by electronic excitation. Experimental spectra together with quantum chemical calculations provide a direct evidence for a ReBr(CO)$_3$ → bpy delocalized charge transfer character of the lowest excited state. Steady-state as well as time-resolved Re L$_3$ spectra of [ReCl(CO)$_3$(bpy)] and [Re(Etpy)(CO)$_3$(bpy)]$^+$ are very similar to those of the Br complex, in agreement with similar (TD) DFT calculated transition energies as well as delocalized excited-state spin densities and charge changes upon excitation.

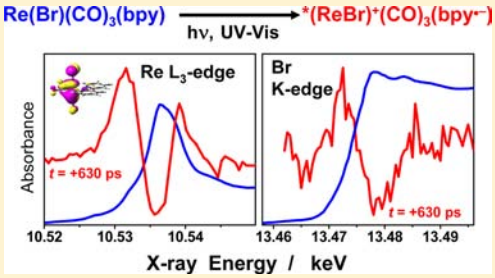

INTRODUCTION

Localization of electronic transitions and electron density redistribution upon excitation are long-standing questions in photophysics of transition metal complexes and also the basis of the textbook classification of excited states, such as metal to ligand charge transfer (MLCT), ligand to ligand charge transfer (LLCT or XLCT), etc. The right description of electronic and structural changes upon light absorption is crucial for predicting excited-state lifetimes, deactivation mechanisms, and reactivity. In the case of *fac*-[ReX(CO)$_3$(α-diimine)]^n chromophores, which are widely used as phosphorescent probes, labels, and electron transfer photosensitizers,[1−6] it is becoming widely accepted that their low-lying emissive "MLCT" excited states should be viewed as delocalized ReX(CO)$_3$ → diimine transitions, where the X → diimine contribution increases with the electron-donating strength (decreasing electronegativity) of the axial ligand X. Pronounced X involvement was indicated for halides (increasing in the order Cl < Br < I), NCS$^-$, and especially amides (NTol$_2^-$, NHPh$^-$) and phosphides (PPh$_2^-$).[7−9] Much of the evidence for the delocalized character of these charge-transfer (CT) transitions emerges from calculations of ground- and excited-state electron densities using density functional theory (DFT).[7,10] Direct experimental evidence is harder to obtain, especially for monatomic halide ligands. The first spectroscopic indication came from the resonance Raman (rR) spectrum of [ReBr(CO)$_3$(bis-*p*tolyl-*N*,*N*-1,4-diazabutadiene)] that showed enhancement of the ν(Re−Br) band as well as of bands due to ν(CO) and diazabutadiene-localized vibrations.[11] Whereas enhancement of the latter two types of Raman bands is characteristic of MLCT transitions, observation of a ν(ReBr) band in the rR spectrum points to a partial depopulation of a Br-localized molecular orbital (MO), affecting the Re−Br bond.

Received: November 27, 2012
Published: April 30, 2013

   dx.doi.org/10.1021/ic3025843 | *Inorg. Chem.* 2013, 52, 5775−5785

Indeed, DFT calculations of [Re(halide)$(CO)_3$(diimine)] complexes have shown that the two highest occupied MOs have a Re-halide π-antibonding character.[7,10] Similarly, rR spectra of [Re(NCS)$(CO)_3$(bis-*i*Pr-*N*,*N*-1,4-diazabutadiene)] and [Re(NCS)$(CO)_3$(bpy)] (bpy = 2,2′-bipyridine) exhibit enhanced bands due to ν(NCS), ν(CO), and diimine vibrations, indicating electron density shift from the whole Re(NCS)$(CO)_3$ moiety to the diimine ligand upon exciting the lowest allowed transition.[8] Time-resolved IR spectra of these two complexes revealed that the ν(CO) and ν(NCS) IR bands shift to higher and lower wavenumbers, respectively, on going from the ground state to the lowest excited state. These shifts were attributed to depopulation of π^*(C≡O) and π(N═C═S) orbitals, respectively, and provide a direct evidence of the delocalized origin of the excited electron in the long-lived triplet state.[8] The extent of this delocalization affects other important photophysical properties such as the singlet−triplet intersystem crossing rate,[7,12,13] triplet-state lifetimes,[14−16] as well as relaxation dynamics.[12,17]

The question of the Re/halide mixed character of the lowest excited state can be addressed directly by time-resolved X-ray absorption spectroscopy (TR-XAS),[18−20] which is an atom-specific technique. The XANES (X-ray absorption near-edge structure) region of ground-state L-edge spectra of metal complexes often shows a band ("white line") due to dipole-allowed transitions of a 2p core electron to empty d orbitals and multiple-scattering (MS) features. Changes of MO occupancy upon optical excitation can result in shifts of the edge onset and/or intensity modulations in the white-line region of the spectrum; in some cases new spectral features emerge or disappear due to addition or removal of electron density to/from MOs involved in X-ray absorption. Indeed, both edge shift and emergence of a new pre-edge spectral band were observed in the time-resolved Ru L_3-edge XANES spectrum of $[Ru(bpy)_3]^{2+}$ measured after excitation with visible light, confirming the assignment of the lowest excited state as ^{3}MLCT, while analysis of the time-resolved EXAFS (extended X-ray absorption fine structure) at higher energies determined the structural differences between the ^{3}MLCT and the ground state.[19,21] Changes in the white-line shape and intensity also have been observed in TR-XAS Pt L_3-edge spectra of $[Pt_2(\mu\text{-}P_2O_5H_2)_4]^{4-}$,[22,23] caused by changes in orbital occupancy and molecular structure upon $d\sigma^* \rightarrow p\sigma$ excitation. Edge shifts to higher energies and appearance of new absorption pre-edge features were observed in halide K-edge TR-XAS measured upon UV laser-pulse induced oxidation of solvated Br^- and I^- ions to Br and I radicals, respectively, that creates a hole in the valence np orbital.[18,24−26]

TR-XAS thus offers a unique opportunity to investigate the character of the lowest excited state of [ReBr$(CO)_3$(bpy)] by separately interrogating electronic changes at the Re and Br atoms by measuring Re L_3-edge and Br K-edge spectra before and after irradiation into the lowest absorption band in the near-UV region. Herein, we present the corresponding XANES spectra and interpret the observed spectral features and their changes upon excitation using time-dependent density functional theory (TD-DFT) calculations of electronic transitions from Re 2p and Br 1s core orbitals into vacant molecular orbitals in the ground state as well as in the lowest triplet state. Experimental details, XANES analysis using multiple scattering theory, and molecular structure determination from the extended X-ray absorption fine structure (EXAFS) part of the spectrum are published elsewhere.[27,28]

METHODS

The complexes [ReX$(CO)_3$(bpy)] (X = Cl, Br) and [Re(Etpy)$(CO)_3$(bpy)]PF_6 (Etpy = 4-Et-pyridine) were prepared by standard procedures and characterized by IR, ^{1}H NMR, and UV−vis spectroscopy.[14,29,30] Measurements were performed in *N*,*N*-dimethylformamide (DMF) or MeCN of a spectroscopic quality (Aldrich). Solutions with concentrations of 100 mM and 30 mM were used for steady-state and time-resolved XAS measurements, respectively.

XAS experiments were performed at the microXAS beamline of the Swiss Light Source (Paul-Scherrer Institut, Villigen, Switzerland) using the experimental setups described in refs 27 and 31. In brief, steady-state spectra were measured in both total fluorescence yield and transmission detection modes. Time-resolved spectra were measured at a 630 ps time delay after 355 nm excitation with a fluence of 60 mJ/cm^2 at a repetition rate of 260 kHz and detected in fluorescence mode.[27,31] A preliminary study using 400 nm, 1 kHz excitation and transmission detection 630 ps after excitation provided virtually identical results (Figure S10, Supporting Information). Experimental details are fully described elsewhere,[27] together with the full-range spectra, error margins, EXAFS analysis, and time-dependencies of transient XAS signals. All data was measured using a Si(111) double-crystal monochromator with an energy bandwidth of 0.014%, providing an energy resolution of 1.5 eV at the Re L_3-edge (10.5 keV) and 1.9 eV at the Br K-edge (13.5 keV).

Electronic structures were calculated by the DFT method using the ADF[32] program package. Pure functionals BP86[33,34] and asymptotically correct SAOP[35] as well as the hybrid functional proposed by Perdew, Burke, and Ernzerhof (PBE0) were used.[36,37] Slater type orbital (STO) basis sets of triple-ζ quality with two polarization functions for Re, Cl, and Br, triple-ζ with one polarization function for C, N, O, and double-ζ with one polarization function for H atoms were employed (inner shells electrons included). Calculations with pure BP86 functional used quadruple-ζ basis set with four polarization functions for Re. Solvent effect was incorporated into DFT calculations by the conductor like screening model (COSMO).[38] Ground-state core transition energies were calculated by TD-DFT at the DFT-optimized geometry (Table S1, Supporting Information). The number of one-electron excited states in the TD-DFT procedure was reduced to the subspace where only the core electrons are excited.[39] This approach has been recently successfully used to interpret L- and K-edge XANES of 3d metal complexes;[39−43] see the Discussion section. Its applicability to L-edge spectra of heavy-metal atoms is supported by the notion that the multiplet effects due to interactions between the core−hole and the excited electron diminish on going down the periodic table because of decreasing overlap of the corresponding radial wave functions and efficient shielding of the 2p core.[44,45]

All calculations included scalar relativistic effects that were approximated by ZORA.[46] Spin−orbit coupling (SO) was treated in three different ways: two-component spin-relativistic approach,[40,47] perturbational approach,[48] and spin-free approach in which SO coupling is neglected. Excited-state triplet−triplet core transitions were calculated at the optimized geometry of the lowest triplet state ^{3}A″ (Table S1) using spin-unrestricted TD-DFT calculation with the PBE0 functional that neglects SO coupling but still includes scalar relativistic effects (ZORA). Absolute values of calculated transition energies are shifted relative to experiment by values ranging from −340 to +160 eV (Re) and 110 to 180 eV (Br), depending on the functional and spin−orbit treatment. This is a common effect in TD-DFT calculations of core excitations, caused by DFT limitations of the core−hole description.[42] Relative energies of transitions responsible for individual pre-edge features, comparisons between different complexes or electronic states, and identification of target orbitals are the most chemically relevant computational outcomes.[42]

RESULTS

Ground-State Spectra. The Re L_3-edge XAS of [ReBr$(CO)_3$(bpy)] in DMF (Figure 1and Figures S1−S3 in the Supporting Information) shows a prominent white line (C)

dx.doi.org/10.1021/ic3025843 | Inorg. Chem. 2013, 52, 5775−5785

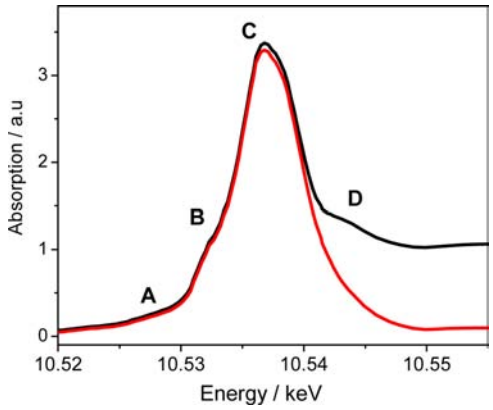

Figure 1. XANES region of the normalized Re L_3-edge XAS spectrum of $[ReBr(CO)_3(bpy)]$ in DMF (black) and the edge-corrected spectrum (red) obtained after subtracting the arctangent ionization edge, as described in the Supporting Information (Figure S1).

with a maximum at 10.537 keV and two pre-edge features A (~10.528 keV, very weak) and B at ~10.532 keV. A shoulder occurs on the high-energy side of the white-line maximum, followed by features D, E, F and EXAFS modulations above 10.6 keV (Figure S2, Supporting Information).[27] Very similar Re L_3-edge spectra were obtained for analogous complexes $[ReCl(CO)_3(bpy)]$ and $[Re(Etpy)(CO)_3(bpy)]^+$ (Figure S3, Supporting Information).

Analysis of the Re L_3-edge XANES spectrum using the MS theory reproduced the white line C, attributing it to $2p_{3/2} \rightarrow 5d$ $Re(CO)_3$-based transitions, whereas the above-ionization feature D was found to have a MS character, mostly involving atoms of the bpy ligand.[27] Higher-lying MS features E and F originate predominantly from scattering at the CO ligands, whereas Br contributes very little.[27,28] In a molecular orbital approach, one can assume that the L_3 XANES spectrum will reflect the energy spectrum of empty MOs with Re 5d and 6s contributions, since only $2p \rightarrow d$ and $2p \rightarrow s$ transitions are dipole allowed. Figure 2 shows DFT-calculated fractional 5d,

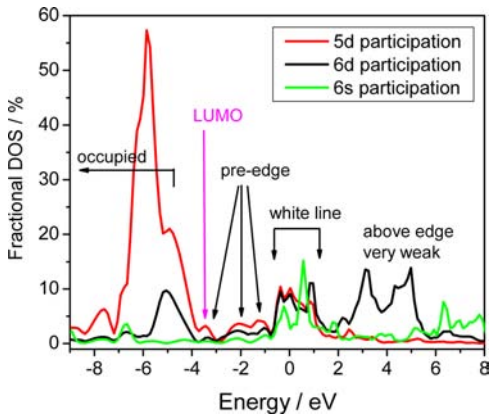

Figure 2. Fractional rhenium 5d, 6d, and 6s densities of states as a function of energy. Calculated by DFT (BP86, vacuum).

6d, and 6s densities of states (DOS). This plot qualitatively indicates that the white line is due to electron excitation from 2p to a group of molecular orbitals between ca. −0.7 and +1.2 eV with a significant, although not predominant, 5d and 6s content. In addition, there is a small 5d participation in the LUMO and in several low-lying unoccupied MOs, which are responsible for the pre-edge feature B. The absorption feature A, lying even lower in energy, cannot be correlated with any calculated empty DOS. Excitation into 6d-containing MOs does not appear to result in strong X-ray absorption since no prominent above-edge features were observed in the experimental spectrum. This likely is caused by a small radial overlap with the core 2p orbital.

Two-component SO TD-DFT calculations of electronic transitions from the $2p_{3/2}$ orbital into empty molecular orbitals are expected to account for XANES better than the DOS since they allow for mixing between one-electron excitations and include spin−orbit coupling. Figure 3 shows the edge-corrected

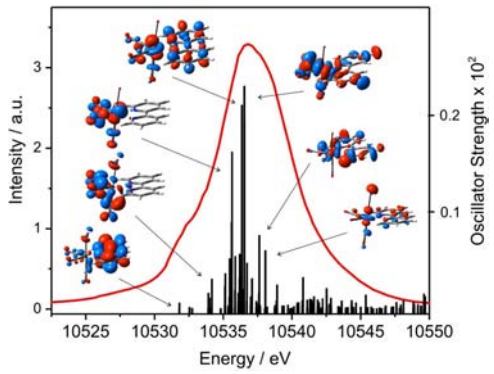

Figure 3. Two-component SO TD-DFT (BP86, vacuum) calculated L_3-edge transitions (black bars, right axis) of $[ReBr(CO)_3(bpy)]$ shown together with the experimental spectrum corrected for the ionization edge (red, left axis). Calculated values are shifted by +118.05 eV. Inset pictures show shapes of target orbitals contributing to the selected transitions by ≥80%. (The Re−Br bond points upward.) Calculated transition energies and oscillator strengths are summarized in Table S2 of the Supporting Information.

experimental spectrum together with calculated transitions, the most prominent ones being characterized by the shapes of the target orbitals of the predominant one-electron excitations.

Figure 3 demonstrates that the two-component SO TD-DFT (BP86, vacuum) calculation corresponds reasonably well to the experimental spectrum, accounting for all the XANES features except the lowest-lying shoulder A. This feature could be tentatively attributed to a partial hole in occupied molecular orbitals originating from spin−orbit mixing of higher-lying triplet states with a $5d^5$ preponderant configuration into the closed-shell $5d^6$ singlet ground state. Indeed, relativistic spin−orbit CASSCF/CASPT2 calculations on $[ReBr(CO)_3(bpy)]$ indicate ca. 0.1% triplet admixture to the ground state.[16] Very similar computational results were obtained for the other two $[ReX(CO)_3(bpy)]^n$ complexes (X = Cl, Etpy), in accordance with the experimental spectra (Figure S3, Supporting Information).

To assess the TD-DFT applicability to L-edge XAS of heavy-metal complexes and ensure that the present TD-DFT spectral interpretation is not an artifact of a particular computational approach, we have tested the effects of the functional, solvent, and spin−orbit treatment. The results are shown in the Supporting Information, Figures S4−S9. It follows that the best match with the experimental spectrum is achieved by two-component spin−orbit calculations using pure functionals BP86 (Figure 3) and SAOP (Figure S4) that give very similar results, even if the asymptotically correct SAOP might be expected to perform better for high-lying virtual orbitals.

dx.doi.org/10.1021/ic3025843 | Inorg. Chem. 2013, 52, 5775−5785

Table 1. TD-DFT (PBE0, COSMO−DMF) Calculated Lowest Energy Transitions from the Re $2p_{x,y}$ (a″) and $2p_z$ (a′) Orbitals of $[ReBr(CO)_3(bpy)]$ in the Electronic Ground State[a]

				target MO fragment contributions (%)					
transition	energy (eV)	oscillator str × 10^2	target MO (% contr)	Re(d)	Re(s)	Br	bpy	CO_{ax}	CO_{eq}
$2^1A'$	10534.2	0.008	73a′ (94)	1		2	94		4
$3^1A'$	10534.8	0.015	47a″ (62)	6			6	17	58
			75a′ (14)	9		1	4	29	42
$3^1A''$	10534.9	0.046	47a″ (67)	6			6	17	58
			75a′ (10)	9		1	4	29	42
$4^1A''$	10534.9	0.030	47a″ (12)	6			6	17	58
			75a′ (67)	9		1	4	29	42
$4^1A'$	10535.0	0.077	75a′ (63)	9		1	4	29	42
$5^1A'$	10535.0	0.104	47a″ (10)	6			6	17	58
			75a′ (63)	9		1	4	29	42
$9^1A'$	10535.7	0.014	76a′ (96)	22		2		24	39
$8^1A''$	10535.7	0.034	76a′ (96)	22		2		24	39
$10^1A'$	10535.8	0.116	77a′ (78)	23	12			25	41
			79a′ (16)	29	6	1		18	27
$9^1A''$	10536.2	0.022	77a′ (75)	23	12			25	41
			79a′ (11)	29	6	1		18	27
$12^1A'$	10536.2	0.045	77a′ (71)	23	12			25	41
			79a′ (13)	29	6	1		18	27
$13^1A'$	10536.3	0.023	48a″ (15)				82		17
			49a″ (25)				17		78
			50a″ (39)	22			6	18	51
$11^1A''$	10536.3	0.026	48a″ (21)				82		17
			49a″ (29)				17		78
			50a″ (21)	22			6	18	51
$14^1A'$	10536.4	0.016	48a″ (15)				82		17
			49a″ (25)				17		78
			50a″ (39)	22			6	18	51
$13^1A''$	10536.4	0.019	48a″ (12)				82		17
			49a″ (17)				17		78
			50a″ (36)	22			6	18	51
$14^1A''$	10536.5	0.010	79a′ (55)	29	6	1		18	27
			75a′ (18)	9		1	4	29	42
$16^1A'$	10536.6	0.188	79a′ (46)	29	6	1		18	27
			50a″ (17)	22		1	6	18	51
$17^1A'$	10536.7	0.259	51a″ (46)	22		2	33	12	24
			52a″ (13)	16			70		7
$16^1A''$	10536.7	0.257	51a″ (46)	22		2	33	12	24
			52a″ (13)	16			70		7
$23^1A'$	10539.1	0.012	51a″ (46)	22		2	33	12	24
			52a″ (13)	16			70		7
$22^1A''$	10539.1	0.012	51a″ (29)	22		2	33	12	24
			52a″ (52)	16			70		7
$30^1A'$	10539.9	0.010	83a′ (82)	2		4	61	6	24
$31^1A'$	10540.1	0.011	85a′ (83)	2		2	55	9	19
$32^1A'$	10540.1	0.012	85a′ (83)	2		2	55	9	19

[a]All calculated transition energies are shifted by −331.9 eV. Only transitions with oscillator strengths larger than 5×10^{-5} are listed. Transitions are expressed as linear combinations of one-electron excitations. Principal target molecular orbitals are characterized by their distribution over the molecule.

Including the DMF solvent into the two-component SO TD-DFT (BP86) calculation using a continuous dielectric model (Figure S5) results in a slightly smaller energy spacing between transitions than the vacuum calculation. Employing a perturbational instead of a two-component approach to spin−orbit coupling (BP86, vacuum) has a very little effect (Figure S6), only slightly changing relative transition intensities. It appears that computationally less demanding perturbational SO TD-DFT is well applicable to XAS. Going from the pure functionals BP86 or SAOP to the hybrid functional PBE0 (perturbational SO, vacuum) does not change the overall spectral pattern and the qualitative transition assignment but narrows the energy range of calculated transitions while still accounting for the features B and C but not for the high-energy shoulder C and for the large white-line width (Figure S7). Surprisingly, neglecting the SO coupling (spin-free TD-DFT, PBE0, vacuum) does not change the calculated XANES spectral pattern, causing only small shifts and changes in relative transition intensities (Figure

dx.doi.org/10.1021/ic3025843 | Inorg. Chem. 2013, 52, 5775−5785

S8). However, L_2 and L_3 edges can no longer be distinguished, and the absolute energy difference between calculated and experimental transitions is much larger than in spin−orbit calculations. Including the solvent into the spin-free PBE0 calculation leads to further small narrowing of the energy span of calculated transitions (Figure S9).

The reasonable match with the low-energy part of the spectrum allowed us to analyze Re L-edge transitions using spin-free TD-DFT (PBE0, COSMO) calculations that provide a more tractable picture of the transitions and their target orbitals than the quantitatively more accurate two-component SO method. The calculated transition energies, oscillator strengths, contributing one-electron excitations, and respective target orbitals are summarized in Table 1. These results, together with target orbitals drawings in Figure 3, show that the pre-edge feature B results from core-to-ligand MLCT transitions into predominantly π^*(bpy) MOs that are closely followed by transitions into a group of π^*(CO) orbitals. These transitions gain intensity from small 5dπ admixtures to the target orbitals, originating from π back bonding. (The feature B encompasses a whole group of 2p → π^*(bpy) transitions, most of which are very weak and thus omitted from Table 1.) The white line and its high-energy shoulder are mostly due to transitions into delocalized molecular orbitals with relatively high participation of 5dσ and 6s orbitals, reaching 20−30% and 6−12%, respectively.

The Br K-edge spectrum of [ReBr(CO)$_3$(bpy)] in DMF (Figure 4) is dominated by the ionization edge (midpoint

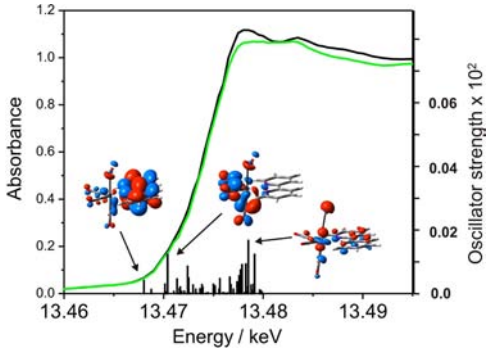

Figure 4. Normalized Br K-edge XAS spectra of [ReBr(CO)$_3$(bpy)] in DMF (black) and MeCN (green), left axis. Two-component SO TD-DFT (BP86, vacuum) calculated Br K-edge transitions are shown as black bars (right axis). Calculated values are shifted by +178 eV to align the strongest transition with the above-edge maximum. Inset pictures show shapes of target orbitals contributing to the selected transitions by ≥80%. (The Re−Br bond points upward.).

13.474 keV) that is preceded by very weak shoulders at its onset and followed by solvent-dependent MS features.[27] Two-component SO TD-DFT calculated transitions at the Br K-edge indicate the presence of bound−bound transitions from the Br 1s orbital to a set of delocalized molecular orbitals with small Br 4p components that confer the oscillator strengths. The low-lying transitions can be viewed as Br(1s)-to-ligand CT, the target ligand being either bpy or, at higher energies, CO. Comparison of Figures 3 and 4 reveals that some of the target orbitals of Re L-edge and Br K-edge transitions are identical. Calculated transitions could account for the modulated onset of the experimental spectrum but direct comparison is not possible because of the lack of any distinct experimental pre-edge features. This is caused by the weakness of Br K-edge transitions, whose oscillator strengths were calculated to be at least 10-times smaller than in the case of Re L_3 edge, in accordance with much smaller calculated Br 4p than Re 5d/6s contributions to unoccupied MOs (Table 1).

Excited-State Spectra. Time-resolved XAS spectra of [ReBr(CO)$_3$(bpy)] at the Re L_3- and Br K-edges are shown in Figures 5 and 6, respectively, while Figure S10 of the

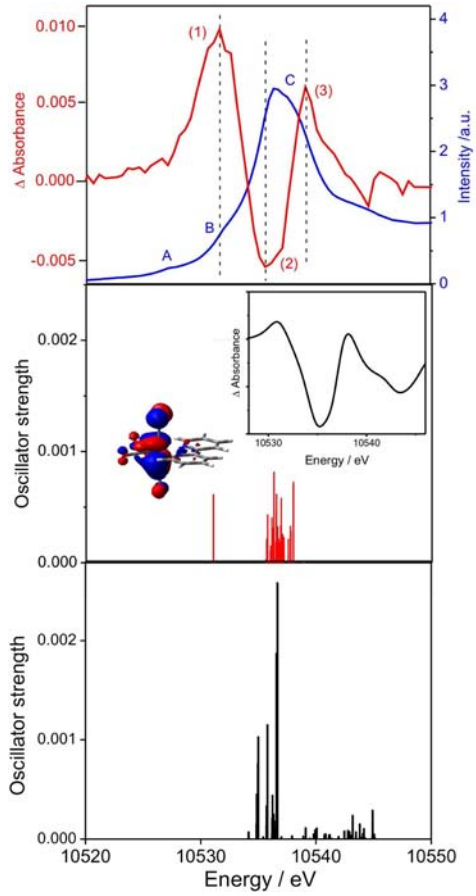

Figure 5. Top: Time-resolved difference Re L_3-edge XAS of [ReBr(CO)$_3$(bpy)] in DMF measured at 630 ps after 355 nm laser pulse excitation (red, left axis). The ground-state spectrum (blue, right axis) is shown for comparison. Middle: TD-DFT (PBE0, COSMO−DMF) calculated triplet−triplet transitions originating from the Re 2p orbital of the a^3A'' excited state. Insets: the shape of the target orbital of the excited-state pre-edge XAS transition and the difference between simulated excited- and ground-state spectra (fwhm = 3 eV). Bottom: TD-DFT (PBE0, COSMO−DMF) calculated transitions from the Re 2p orbital in the ground state. All calculated transition energies are shifted by −331.9 eV. (The higher density of calculated excited-state transitions (middle) is due to the spin-unrestricted treatment that calculates α and β spin−orbitals at slightly different energies.) Calculated excited-state transitions and their target orbitals are summarized in Table 2.

Supporting Information compares the Re spectra of all three [ReL(CO)$_3$(bpy)]^n complexes (L = Cl, Br, Etpy). These figures show the XAS signal obtained at 630 ps after 355 nm laser-pulse excitation minus the signal measured before excitation. The positive features are attributed to the lowest excited state a^3A'' that is fully equilibrated on this time scale,[12] while the negative bands ("bleaches") are due to ground-state depletion. (Decay kinetics of the transient XAS intensities and analysis of the EXAFS region of the excited-state spectrum are presented

dx.doi.org/10.1021/ic3025843 | Inorg. Chem. 2013, 52, 5775−5785

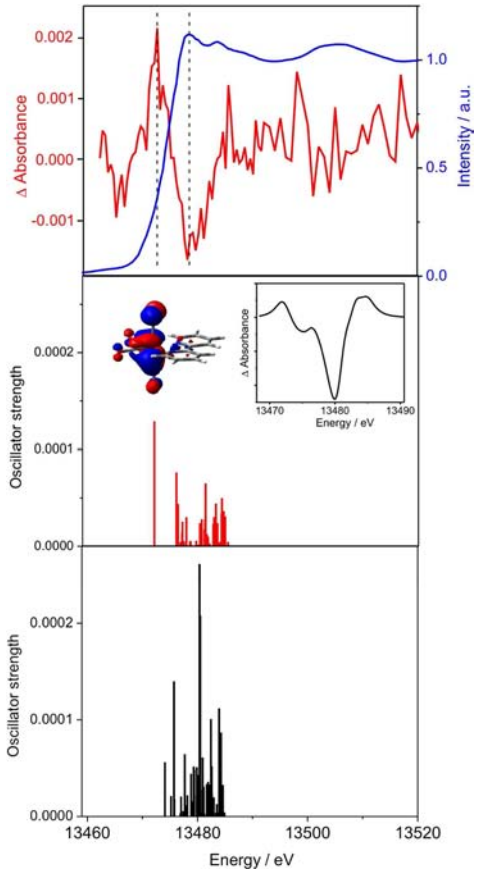

Figure 6. Top: Time-resolved difference Br K-edge XAS of $[ReBr(CO)_3(bpy)]$ in DMF measured at 630 ps after 355 nm laser pulse excitation (red, left axis). The ground-state spectrum (blue, right axis) is shown for comparison. Middle: TD-DFT (PBE0, COSMO–DMF) calculated triplet–triplet transitions originating from the Br 1s orbital of the a^3A'' excited state. Insets: the shape of the target orbital of the excited-state pre-edge XAS transition and the difference between simulated excited- and ground-state spectra (fwhm = 3 eV). Bottom: TD-DFT (PBE0, COSMO–DMF) calculated transitions from the Br 1s orbital in the ground state. All calculated transition energies are shifted by +119 eV.

elsewhere.[27]) In the XANES region, the Re L_3 TR-XAS of $[ReBr(CO)_3(bpy)]$ (Figure 5) shows a prominent new excited-state feature (1) at ~10.531 keV, that is ca. 5.7 eV below the ground-state white line maximum (C). The minimum (2) at about 10.535 keV and a broad maximum (3) centered at around 10.539 keV are due to an excitation-induced diminished intensity of the feature B, white-line shift to higher energies, and ionization edge shift by ca. 0.5 eV[27] to higher energies. The Br K-edge spectrum (Figure 6) exhibits similar behavior: a new pre-edge absorption feature arises at 13.472 keV, followed by a minimum (ground-state bleached absorption) at ~13.479 keV, and a new edge-like signal at a 13.482 keV midpoint.

TD-DFT calculations of excited-state XAS spectra were performed on the UKS-optimized geometry of the lowest a^3A'' excited state (Table S1), which was shown[27] to reproduce well the excited-state EXAFS pattern. Electronic transitions of the a^3A'' state originating from the Re 2p and Br 1s orbitals were calculated by TD-DFT (PBE0, COSMO–DMF). Calculated Re transitions and analysis of their target spin–orbitals are presented in Table 2. Spin–orbit coupling was neglected since neither 2-component nor perturbational SO treatments are available for TD-DFT calculations of open-shell systems, such as electronic excited states. The hybrid functional PBE0 was chosen because pure functionals do not provide a good description of CT excited states of metal-diimine complexes, unrealistically diminishing the HOMO–LUMO gap.[10,49,50] The calculated excited-state transitions are shown in Figures 5 and 6 (middle) together with the preponderant target orbital of the transition responsible for the excited-state pre-edge features. It follows that, despite crude approximations involved, TD-DFT calculations reproduce well the XAS changes between the lowest excited and the ground state. The calculated difference between the Re pre-edge band (1) and the excited-state white line maximum (3), 7 eV, is in good agreement with the experimental value of ~8 eV. Excited-state calculations identified the target spin–orbital of the excited-state pre-edge features of both Re L- and Br K-edge spectra as β45a″ that is created by depopulation of the ground-state a″ HOMO-1 upon optical excitation (Table 2). The 48% Re 5d and 17% Br (4p) contributions to this spin orbital enable rather high oscillator strengths of the Re(2p) → β45a″ and Br(1s) → β45a″ transitions, making the pre-edge features in both the Re and Br excited-state XAS spectra clearly observable. The calculation also points to the decrease of the B-feature intensity and its ~1.4 eV shift to higher energies, in accordance with the experiment (compare transitions to the $2^1A'$ and $2^3A'$ states in Tables 1 and 2, respectively.)

DISCUSSION

XANES spectra are usually interpreted in the framework of multiplet theory[44] or single-electron multiple scattering theory.[51,52] While the former is important for open-shell complexes of the first-row 3d transition elements, the latter is effective for heavier 4d and 5d systems and accounts also for purely structural resonances appearing at higher energies. MS theory (shell-by-shell simulation) assigns[27] the $[ReBr(CO)_3(bpy)]$ white-line C to transitions from $2p_{3/2}$ into 5d-based orbitals and the D-F features to multiple scattering, without providing information about the character of the target orbitals. It does not account for the pre-edge features A and B.[27]

DFT and TD-DFT calculations offer a complementary approach to MS. They interpret the near-edge XAS features as transitions from the core orbitals (1s and 2p for K- and L-edges, respectively) to empty molecular orbitals. By using the MO picture, this approach provides an insight into bonding and covalency in metal complexes in common chemical terms and informs us on the nature and energies of unoccupied MOs, including high-lying ones that can be photochemically relevant. TD-DFT adapted for core electron excitations[39] has been successfully used to account for K- and L-edge spectra of light elements such as Cl and Ti in $TiCl_4$ without[39] and with[40] spin–orbit coupling, Cl K-edge spectra of various metal chlorides,[53] as well as metal (V, Cr, Mn) $L_{2,3}$- and oxygen K-edges spectra of a series of oxochlorides.[43] Other TD-DFT studies reproduced metal K-edge spectra of series of Mn[41] and Fe[42] complexes and examined the dependence on the functional, solvent, and scalar relativistic effects. These studies have demonstrated that relativistic spin–orbit TD-DFT calculations deal well with 2p core hole −3d electron interaction, coupling between one-electron excitations, as well as covalency, whose treatment is oversimplified in multiplet theories.

Herein, we apply relativistic spin–orbit TD-DFT to L_3- and K-edge XAS of two atoms, Re and Br, respectively, in both the

dx.doi.org/10.1021/ic3025843 | Inorg. Chem. 2013, 52, 5775–5785

Table 2. TD-DFT (PBE0, COSMO−DMF) Calculated Lowest Energy Transitions from the Re $2p_{x,y}$ (a″) and $2p_z$ (a′) Orbitals of $[ReBr(CO)_3(bpy)]$ in the a^3A'' Electronic State[a]

				target MO fragment contributions (%)					
transition	energy (eV)	oscillator str × 10^2	target MO (% contr)	Re(d)	Re(s)	Br	bpy	CO_{ax}	CO_{eq}
$1^3A'$	10531.0	0.062	β45a″ (96)	48		17	8	14	9
$2^3A''$	10531.0	0.061	β45a″ (96)	48		17	8	14	9
$2^3A'$	10535.6	0.003	β73a′ (73)	1		1	87		8
$4^3A'$	10535.7	0.021	α74a′ (43)	2		3	54	12	24
			α78a′ (24)	33	7	10	4	17	17
$6^3A''$	10535.7	0.017	α46a″ (83)	9		1	4	46	31
$6^3A'$	10535.7	0.043	α74a′ (28)	2		3	54	12	24
			α46a″ (26)	9		1	4	46	31
			α78a′ (14)	33	7	10	4	17	17
$7^3A'$	10536.0	0.011	β75a′ (26)	3		1	38	41	11
			β74a′ (20)	3		3	54	12	24
			β76a′ (15)	23			6	17	58
$8^3A'$	10536.0	0.015	β75a′ (30)	3		1	38	41	11
			β74a′ (24)	3		3	54	12	24
			β76a′ (20)	23			6	17	58
$10^3A'$	10536.1	0.015	α76a′ (54)	23			6	17	58
			β46a″ (33)	7		1	3	24	55
$10^3A''$	10536.1	0.014	α76a′ (76)	23		2	5	17	45
$11^3A'$	10536.1	0.041	α76a′ (68)	23			6	17	58
			β46a″ (18)	7		1	3	24	55
$11^3A''$	10536.2	0.031	β76a′ (68)	23		2	5	17	45
$13^3A'$	10536.3	0.082	β76a′ (61)	23			6	17	58
			β78a′ (11)	34	12	1	2	15	16
$16^3A'$	10536.5	0.019	β77a′ (92)	21				22	51
$13^3A''$	10536.5	0.046	β77a′ (81)	21				22	51
$17^3A'$	10536.5	0.062	β77a′ (73)	21				22	51
$18^3A'$	10536.6	0.033	α49a″ (41)	16			7	12	60
			α47a″ (40)	1			87		10
$15^3A''$	10536.6	0.031	α49a″ (44)	16			7	12	60
			α47a″ (40)	1			87		10
$19^3A'$	10536.7	0.022	α78a′ (49)	33	7	10	4	17	6
			α74a′ (45)	2		3	54	12	24
$20^3A'$	10536.8	0.019	α78a′ (50)	33	7	10	4	17	17
			α74a′ (36)	2		3	54	12	24
$17^3A''$	10536.8	0.009	α48a″ (66)	1			7	12	60
			α47a″ (23)	1			2	23	67
$22^3A'$	10536.9	0.034	β78a′ (50)	34	12	11	6	15	16
			β74a′ (36)	4		2	61	24	6
$23^3A'$	10536.9	0.018	β78a′ (33)	34	12	8	6	15	16
			β47a″ (26)	1			2	23	67
			β74a′ (23)	4		2	61	24	6
$21^3A''$	10536.9	0.010	β47a″ (71)	1			85	1	11
			β49a″ (15)	23			19	15	43
$24^3A'$	10536.9	0.058	β47a″ (45)	1			85	1	11
			β78a′ (19)	34	12	11	6	15	16
$25^3A'$	10537.0	0.008	α75a′ (33)	2		1	43	33	14
			α74a′ (16)	3			38	41	10
$24^3A''$	10537.0	0.011	β48a″ (76)	1			85	1	11
			β49a″ (15)	19			20	15	43
$27^3A'$	10537.1	0.026	β48a″ (68)	1			85	1	11
			β49a″ (14)	19			20	15	43
$29^3A'$	10537.1	0.012	α75a′ (61)	2		1	43	33	14
			α74a′ (17)	3			38	41	10
$31^3A'$	10537.6	0.021	β49a″ (54)	19			20	15	43
			β47a″ (26)	1			85	1	11
$30^3A''$	10537.7	0.033	α51a″ (91)	28		1	30	2	15
$32^3A'$	10537.8	0.029	α51a″ (87)	28		1	30	2	15
$33^3A''$	10538.0	0.070	β51a″ (95)	28		2	28	4	12

dx.doi.org/10.1021/ic3025843 | Inorg. Chem. 2013, 52, 5775−5785

Table 2. continued

				target MO fragment contributions (%)					
transition	energy (eV)	oscillator str × 10^2	target MO (% contr)	Re(d)	Re(s)	Br	bpy	CO_{ax}	CO_{eq}
$33^3A'$	10538.0	0.073	β51a″ (91)	28		2	28	4	12

[a]All calculated transition energies are shifted by −331.9 eV. Only transitions with oscillator strengths larger than 5×10^{-5} are listed. Transitions are expressed as linear combinations of one-electron excitations. Principal target spin-orbitals are characterized by their distribution over the molecule.

ground state and the lowest electronic excited state of $[ReBr(CO)_3(bpy)]$. The best results on the Re L_3-edge were obtained using the pure functionals BP86 and SAOP. Using the hybrid functional PBE0 instead of BP86 (and/or including the solvent) shifts lowest-lying $Re(2p_{3/2}) \rightarrow \pi^*(bpy)$ MLCT transitions up in energy relative to higher-lying transitions with a larger metal participation, decreasing the energy span of calculated transitions and underestimating the width of the ground-state XANES spectrum. However, the qualitative interpretation of the XANES features in terms of the characters of the underlying transitions and their target orbitals is virtually the same, regardless of the functional used, BP86 or PBE0, see Figure 3 and Table 1. This behavior contrasts calculations of optical spectra, where BP86 severely underestimates the HOMO−LUMO energy gap and the use of hybrid functionals together with solvation is essential to model low-energy UV−vis absorption spectra arising from MLCT transitions of valence electrons.[10,49] It also contrasts TD-DFT calculations of K-edge spectra of Mn complexes with polypyridine ligands, where correct relative energies and band intensities of quadrupole-allowed 1s → 3d and MLCT transitions are obtained only upon including the Hartree−Fock exchange (i.e., using hybrid functionals).[41] It is noteworthy that neglecting SO coupling does not qualitatively alter the calculated spectra (Figures S7 and S8, Supporting Information), apparently due to a small radial overlap of the core−hole and 5d wave functions. This allowed us using spin-free TD-DFT (PBE0) calculations to compare XAS transitions in the lowest excited state and the ground state.

The Re L_3-edge XAS intensity is gained from the 5d and 6s contributions to the target molecular orbitals, as is indicated by the calculated 5d and 6s DOS spectra (Figure 2) that roughly reflect the B and C spectral features. However, data in Table 1 show that the calculated oscillator strengths cannot be simply correlated with 5d and 6s contents and that the detailed character of the transition and target orbitals involved matter as well. Analysis of the computational results (Figure 3, Table 1) shows that the Re XANES features arise from five groups of transitions: $Re(2p_{3/2}) \rightarrow \pi^*(bpy)$ MLCT and, at slightly higher energies, $Re(2p_{3/2}) \rightarrow \pi^*(CO)$ MLCT in the energy range of the feature B. The d-participation in the respective target orbitals is rather low, 1−9%. Higher-lying transitions have larger d participations, typically 20−30%: $Re(2p_{3/2}) \rightarrow \pi^*(Re(CO)_3)$ MLCT/MC (MC = metal-centered) transitions that contribute to the low-energy part of C, followed by $Re(2p_{3/2}) \rightarrow \sigma^*/\pi^*(Re(CO)_3)$ and $Re(2p_{3/2}) \rightarrow \sigma^*/\pi^*(Re(CO)_3(bpy))$ MC/MLCT transitions, which give rise to the feature C and its high-energy shoulder, respectively. The d-character is spread over many unoccupied MOs: the 5dπ orbitals contribute to the $\pi^*(bpy)$, $\pi^*(CO)$, and $\pi^*(Re(CO)_3)$ MO sets as a consequence of π back bonding, while mixing between Re 5d and 6s orbitals and various combinations of σ and π^* ligand orbitals in high-lying MOs is due to strong covalent bonding. Table 1 and Figure 3 show that delocalization of these metal−ligand σ^*/π^* orbitals spreads over the $Re(CO)_3$ fragment at lower energies while the highest calculated MO's are delocalized over the whole $Re(CO)_3(bpy)$ unit. Contrary to qualitative expectations, we have no evidence for the presence of two distinct e_g-like predominantly 5d orbitals. Instead, the 5d-contributions to high-lying unoccupied MOs never exceeds 30%. These bonding characteristics seem to be typical for mixed-ligand heavy-metal carbonyls.[54−57]

The width and structure of the experimentally measured white line, together with DFT calculations (Figure 2, Table 1) show that the group of MOs with a significant (20−30%) Re-d content starts at about 3 eV above the $\pi^*(bpy)$ LUMO while the set of MOs with a partial Re ligand σ^* character emerge ca. 1 eV higher. Given that the lowest optical MLCT transitions to the LUMO occur at about 3.1 eV,[10,16,49] it follows that direct excitation of valence electrons into σ^*/π^* MOs would require at least 7 eV, i.e. ≤175 nm vacuum-UV light. Hence, UV (313−250 nm; 4−5 eV) induced photochemical bond-dissociation in $[ReCl(CO)_3(bpy)]$[58−60] has to involve excitation into the upper part of the $\pi^*(bpy)$ set and/or into the $\pi^*(Re(CO)_3)$ MO sets. These optically populated MLCT excited states are either reactive themselves or undergo conversion to dissociative σ^* states at highly distorted geometries in the course of the photochemical reaction.[61,62] It is also important to note that neither of the calculated unoccupied orbitals possess a strong Br character, explaining the virtual absence of pre-edge transitions in the Br K-edge XAS.

Compared with that of the ground state, excited-state Re L_3 and Br K spectra show shifts of the Re white-line and of both absorption edges to higher energies, together with the emergence of new intense pre-edge features. Taken together, this behavior provides a compelling qualitative evidence of a mixed Re/Br character of the lowest excited state: The shifts indicate electron depopulation of both atoms and the new pre-edge absorptions reveal creation of a hole in a molecular orbital of significant Re 5d as well as Br 4p characters, that is a Re/Br mixed origin of the excited electron. This delocalized $ReBr(CO)_3 \rightarrow$ bpy CT character of the a^3A'' lowest excited state is clearly visualized by the spin-density distribution (Figure 7 and Table S3) and the electron-density difference

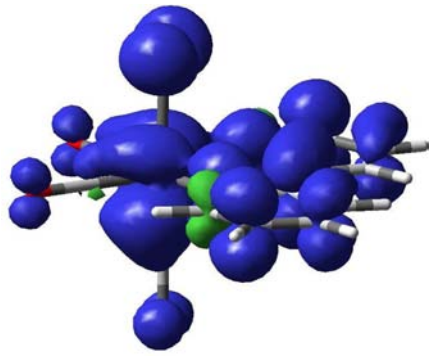

Figure 7. DFT (PBE0/PCM-DMF) calculated Mulliken spin density distribution in the lowest triplet state of $[ReBr(CO)_3(bpy)]$.

dx.doi.org/10.1021/ic3025843 | Inorg. Chem. 2013, 52, 5775−5785

map (Figure S11) calculated at the optimized a^3A'' and ground-state geometries, respectively. The change of the Br K-edge spectrum upon excitation qualitatively resembles the spectral changes found upon oxidation of Br^- and I^- ions in solution,[24−26] in accordance with the presumed partial oxidation of the Br^- ligand in excited $[ReBr(CO)_3(bpy)]$; the excited-state and solvated Br^0 pre-edge XAS bands occur at similar energies of 13.472 and 13.473 keV,[24] respectively. The Re L_3-edge changes are similar to those[21] of Ru L_3-edge TR-XAS measured upon MLCT excitation of $[Ru(bpy)_3]^{2+}$.

TD-DFT calculations reproduce very well the changes of both Re and Br spectra upon optical excitation and identify the common target orbital of the intense Re and Br pre-edge features as lowest unoccupied spin−orbital β45a″ that has arisen from electron excitation from the ground-state doubly occupied HOMO-1, Table 2. Comparison of the ground- and excited-state calculations (Tables 1, 2) agrees with the observed 1−2 eV shift of Re L_3 transitions to higher energies upon optical excitation (e.g., 1.4 eV for the directly comparable $2^3A'$ a $2^1A'$ 2p → π^*(bpy) MLCT) and reveals a more extensive mixing of one-electron excitations in the excited-state transitions and more extensive delocalization of excited-state spin−orbitals over the whole $Re(CO)_3(bpy)$ unit (but not the Br ligand). It is also interesting to note the change of the orbital character upon electron removal from the parent HOMO-1: 44% Re, 30% Br, 22% CO in HOMO-1 vs 48% Re, 17% Br, and 23% CO in β45a″.

The Re L_3-edge TR-XAS spectra of the three investigated complexes $[ReX(CO)_3(bpy)]^n$ (X = Cl, Br, Etpy) are very similar (Figure S10), despite the X → bpy contribution decreasing from Br to Cl and vanishing for Etpy. This result is corroborated by calculated differences of the Re localized charge between the excited state and the ground state, which are almost independent of X: 0.44 (Cl), 0.42 (Br), and 0.38 e^- (Etpy), in accordance with the nearly identical XAS edge shifts observed upon excitation, Table S4. The Re localized spin-density in the a^3A'' state (Table S3) also is very similar in the three complexes, increasing only very little on going from Br (0.66) to Cl (0.69), and Etpy (0.76), as the X → bpy CT contribution diminishes. These results indicate that the Re center undergoes comparable electronic depopulation on excitation, regardless the character of the ligand X. Apparently, the diminishing X participation in the charge transfer to bpy is compensated by adjustments of Re → CO π back bonding and σ-donation.

CONCLUSIONS

XANES spectra of heavy-metal mixed-ligand carbonyl complexes can be analyzed using DFT and TD-DFT calculations, providing important information on their electronic structure, covalency, nature of high-lying unoccupied molecular orbitals, and, in the case of time-resolved spectra, on electronic redistribution upon optical excitation. In particular, the ground-state Re L_3 XANES spectrum of $[ReBr(CO)_3(bpy)]$ shows pre-edge features due to core-to-ligand MLCT transitions from Re $2p_{3/2}$ to predominantly π^*(bpy) and π^*(CO) MOs with 1−9% 5d character, followed by transitions to MOs with a larger (20−30%) 5d-content: $Re(2p_{3/2}) \rightarrow \pi^*(Re(CO)_3)$, $Re(2p_{3/2}) \rightarrow \sigma^*/\pi^*(Re(CO)_3)$ and, at higher energies, $Re(2p_{3/2}) \rightarrow \sigma^*/\pi^*(Re(CO)_3(bpy))$. The dense manifold of mixed-character σ^*/π^* MOs starts about 7 eV above the HOMO. As is typical for heavy-metal mixed-ligand carbonyls, the 5d character is distributed over many unoccupied MOs, contributing maximally 30% to any single unoccupied MO, due to a highly covalent character of the metal−ligand bonding. The Br K edge XANES is dominated by the ionization edge and multiple scattering features. Time-resolved XANES spectra at two molecular sites, namely Re L_3- and Br K-edges show the emergence of new pre-edge features and high-energy shifts, indicating partial oxidation of both centers upon UV−vis excitation. They provide an unequivocal evidence for the delocalized $ReBr(CO)_3$ → bpy character of the lowest excited state, i.e. for MLCT/XLCT mixing. TD-DFT analysis informs us on the character of the unoccupied spin−orbitals in the lowest electronic excited state, namely on their energy changes and larger delocalization compared with the ground state. Observed spectral changes are well accounted for by TD-DFT and DFT calculations that also identify the vacated molecular orbital and describe the electron-density redistribution upon excitation. DFT and TD-DFT interpretation of the XAS spectra of 5d organometallics is facilitated by a small radial overlap between the core hole and target molecular orbitals wave functions, which diminishes multiplet effects resulting from interactions between the core−hole and the excited electron. Time-resolved X-ray absorption emerges as a unique technique informing us on electronic changes at monatomic halide ligands.

ASSOCIATED CONTENT

Supporting Information

Deconvolution of the ground-state Re L_3-edge XANES spectrum into three Lorentzians and an arctangent edge function, figures showing full energy range Re L_3-edge XAS of $[ReBr(CO)_3(bpy)]$, comparison of ground- and time-resolved XANES spectra of $[ReBr(CO)_3(bpy)]$ (L = Cl, Br, Etpy), comparison of Re L_3-edge transitions calculated by different functionals (BP86, SAOP, PBE0) with/without the solvent and different ways of spin−orbit treatment (two-component, perturbational, spin-free), and electron-density redistribution upon excitation into the lowest triplet. Tables: DFT-calculated ground- and excited-state bond lengths and angles, Re energies and oscillator strengths of Re L_3 transitions calculated by 2-component SO TD-DFT, spin-density distribution in the a^3A'' excited state, and changes of charge distribution upon excitation. This material is available free of charge via the Internet at http://pubs.acs.org.

AUTHOR INFORMATION

Corresponding Author

*E-mail: stanislav.zalis@jh-inst.cas.cz (S.Z.), chris.milne@psi.ch (C.J.M.), a.vlcek@qmul.ac.uk (A.V.).

Present Addresses

[‖]Chris J. Milne: SwissFEL, Paul-Scherrer-Institut, CH-5232 Villigen, Switzerland.

[⊥]Amal El Nahhas: Department of Chemical Physics, Lund University, Box 124, 22100 Lund, Sweden.

[#]Renske M. van der Veen: Arthur Amos Noyes Laboratory of Chemical Physics, California Institute of Technology, Pasadena, CA 91125, USA.

Notes

The authors declare no competing financial interest.

ACKNOWLEDGMENTS

We thank Prof. Majed Chergui (EPFL) for helpful and stimulating discussions, as well as for critical reading of the

manuscript. Financial support was provided by the Swiss NSF through the NCCR MUST "Molecular ultrafast science and technology" and contracts 200020-127231/1 and 200020-135502, QMUL, Czech Republic Ministry of Education grant LD11086, and European collaboration programs COST Actions D35, CM1002 and CM1012, as well as ESF-DYNA.

REFERENCES

(1) Vlček, A., Jr. *Top. Organomet. Chem.* **2010**, *29*, 73−114.
(2) Kumar, A.; Sun, S.-S.; Lees, A. J. *Top. Organomet. Chem.* **2010**, *29*, 1−35.
(3) Shih, C.; Museth, A. K.; Abrahamsson, M.; Blanco-Rodriguez, A. M.; Di Bilio, A. J.; Sudhamsu, J.; Crane, B. R.; Ronayne, K. L.; Towrie, M.; Vlček, A., Jr.; Richards, J. H.; Winkler, J. R.; Gray, H. B. *Science* **2008**, *320*, 1760−1762.
(4) Blanco-Rodríguez, A. M.; Di Bilio, A. J.; Shih, C.; Museth, A. K.; Clark, I. P.; Towrie, M.; Cannizzo, A.; Sudhamsu, J.; Crane, B. R.; Sýkora, J.; Winkler, J. R.; Gray, H. B.; Záliš, S.; Vlček, A., Jr. *Chem.—Eur. J.* **2011**, *17*, 5350−5361.
(5) Lo, K. K.-W. *Top. Organomet. Chem.* **2010**, *29*, 115−158.
(6) Lo, K. K.-W.; Louie, M.-W.; Zhang, K. Y. *Coord. Chem. Rev.* **2010**, *254*, 2603−2622.
(7) Cannizzo, A.; Blanco-Rodríguez, A. M.; Nahhas, A.; Šebera, J.; Záliš, S.; Vlček, A., Jr.; Chergui, M. *J. Am. Chem. Soc.* **2008**, *130*, 8967−8974.
(8) Blanco-Rodríguez, A. M.; Gabrielsson, A.; Motevalli, M.; Matousek, P.; Towrie, M.; Šebera, J.; Záliš, S.; Vlček, A., Jr. *J. Phys. Chem. A* **2005**, *109*, 5016−5025.
(9) Gabrielsson, A.; Busby, M.; Matousek, P.; Towrie, M.; Hevia, E.; Cuesta, L.; Perez, J.; Záliš, S.; Vlček, A., Jr. *Inorg. Chem.* **2006**, *45*, 9789−9797.
(10) Vlček, A., Jr.; Záliš, S. *Coord. Chem. Rev.* **2007**, *251*, 258−287.
(11) Stor, G. J.; Stufkens, D. J.; Oskam, A. *Inorg. Chem.* **1992**, *31*, 1318−1319.
(12) El Nahhas, A.; Cannizzo, A.; van Mourik, F.; Blanco-Rodríguez, A. M.; Záliš, S.; Vlček, A., Jr.; Chergui, M. *J. Phys. Chem. A* **2010**, *114*, 6361−6369.
(13) El Nahhas, A.; Consani, C.; Blanco-Rodríguez, A. M.; Lancaster, K. M.; Braem, O.; Cannizzo, A.; Towrie, M.; Clark, I. P.; Záliš, S.; Chergui, M.; Vlček, A., Jr. *Inorg. Chem.* **2011**, *50*, 2932−2943.
(14) Rossenaar, B. D.; Stufkens, D. J.; Vlček, A., Jr. *Inorg. Chem.* **1996**, *35*, 2902−2909.
(15) Stufkens, D. J.; Vlček, A., Jr. *Coord. Chem. Rev.* **1998**, *177*, 127−179.
(16) Heydová, R.; Gindensperger, E.; Romano, R.; Sýkora, J.; Vlček, A., Jr.; Záliš, S.; Daniel, C. *J. Phys. Chem. A* **2012**, *116*, 11319−11329.
(17) Blanco-Rodríguez, A. M.; Towrie, M.; Clark, I. P.; Záliš, S.; Vlček, A., Jr. *manuscript in preparation.*
(18) Bressler, C.; Abela, R.; Chergui, M. *Z. Kristallogr.* **2008**, *223*, 307−321.
(19) Saes, M.; Bressler, C.; Abela, R.; Grolimund, D.; Johnson, S. L.; Heimann, P. A.; Chergui, M. *Phys. Rev. Lett.* **2003**, *90*, 047403.
(20) Bressler, C.; Chergui, M. *Chem. Rev.* **2004**, *104*, 1781−1812.
(21) Gawelda, W.; Johnson, M.; de Groot, F. M. F.; Abela, R.; Bressler, C.; Chergui, M. *J. Am. Chem. Soc.* **2006**, *128*, 5001−5009.
(22) van der Veen, R. M.; Milne, C. J.; El Nahhas, A.; Lima, F. A.; Pham, V.-T.; Best, J.; Weinstein, J. A.; Borca, C. N.; Abela, R.; Bressler, C.; Chergui, M. *Angew. Chem., Int. Ed.* **2009**, *48*, 2711−2714.
(23) van der Veen, R. M.; Kas, J. J.; Milne, C. J.; Pham, V.-T.; El Nahhas, A.; Lima, F. A.; Vithanage, D. A.; Rehr, J. J.; Abela, R.; Chergui, M. *Phys. Chem. Chem. Phys.* **2010**, *12*, 5551−5561.
(24) Elles, C. G.; Shkrob, I. A.; Crowell, R. A.; Arms, D. A.; Landahl, E. C. *J. Chem. Phys.* **2008**, *128*, 061102.
(25) Pham, V.-T.; Gawelda, W.; Zaushitsyn, Y.; Kaiser, M.; Grolimund, D.; Johnson, S. L.; Abela, R.; Bressler, C.; Chergui, M. *J. Am. Chem. Soc.* **2007**, *129*, 1530−1531.
(26) Pham, V.-T.; Penfold, T. J.; van der Veen, R. M.; Lima, F.; El Nahhas, A.; Johnson, S. L.; Beaud, P.; Abela, R.; Bressler, C.; Tavernelli, I.; Milne, C. J.; Chergui, M. *J. Am. Chem. Soc.* **2011**, *133*, 12740−12748.
(27) El Nahhas, A.; van der Veen, R. M.; Penfold, T. J.; Pham, V.-T.; Lima, F. A.; Abela, R.; Blanco-Rodríguez, A. M.; Záliš, S.; Vlček, A., Jr.; Tavernelli, I.; Rothlisberger, U.; Milne, C. J.; Chergui, M. *J. Phys. Chem. A* **2013**, *117*, 361−369.
(28) Penfold, T. J.; Tavernelli, I.; Milne, C. J.; Reinhard, M.; El Nahhas, A.; Abela, R.; Rothlisberger, U.; Chergui, M. *J. Chem. Phys.* **2013**, *138*, 014104.
(29) Hino, J. K.; Della Ciana, L.; Dressick, W. J.; Sullivan, B. P. *Inorg. Chem.* **1992**, *31*, 1072−1080.
(30) Worl, L. A.; Duesing, R.; Chen, P.; Della Ciana, L.; Meyer, T. J. *J. Chem. Soc., Dalton Trans.* **1991**, 849−858.
(31) Lima, F. A.; Milne, C. J.; Amarasinghe, D. C. V.; Rittmann-Frank, M. H.; van der Veen, R. M.; Reinhard, M.; Pham, V.-T.; Karlsson, S.; Johnson, S. L.; Grolimund, D.; Borca, C. N.; Huthwelker, T.; Janousch, M.; van Mourik, F.; Abela, R.; Chergui, M. *Rev. Sci. Instrum.* **2011**, *82*, 063111.
(32) *ADF2012.01, SCM, Theoretical Chemistry*; Vrije Universiteit: Amsterdam, The Netherlands, http://www.scm.com.
(33) Becke, A. D. *Phys. Rev. A* **1988**, *38*, 3098.
(34) Perdew, J. P. *Phys. Rev. A* **1986**, *33*, 8822.
(35) Schipper, P. R. T.; Gritsenko, O. V.; van Gisbergen, S. J. A.; Baerends, E. J. *J. Chem. Phys.* **2000**, *112*, 1344−1352.
(36) Perdew, J. P.; Burke, K.; Ernzerhof, M. *Phys. Rev. Lett.* **1996**, *77*, 3865−3868.
(37) Adamo, C.; Barone, V. *J. Chem. Phys.* **1999**, *110*, 6158−6170.
(38) Klamt, A. *J. Phys. Chem.* **1995**, *99*, 2224−2235.
(39) Stener, M.; Fronzoni, G.; de Simone, M. *Chem. Phys. Lett.* **2003**, *373*, 115−123.
(40) Fronzoni, G.; Stener, M.; Decleva, P.; Wang, F.; Ziegler, T.; van Lenthe, E.; Baerends, E. J. *Chem. Phys. Lett.* **2005**, *416*, 56−63.
(41) Roemelt, M.; Beckwith, M. A.; Duboc, C.; Collomb, M.-N.; Neese, F.; DeBeer, S. *Inorg. Chem.* **2012**, *51*, 680−687.
(42) DeBeer George, S.; Petrenko, T.; Neese, F. *J. Phys. Chem. A* **2008**, *112*, 12936−12943.
(43) Fronzoni, G.; Stener, M.; Decleva, P.; de Simone, M.; Coreno, M.; Franceschi, P.; Furlani, C.; Prince, K. C. *J. Phys. Chem. A* **2009**, *113*, 2914−2925.
(44) de Groot, F. *Coord. Chem. Rev.* **2005**, *249*, 31−63.
(45) Alperovich, I.; Smolentsev, G.; Moonshiram, D.; Jurss, J. W.; Concepcion, J. J.; Meyer, T. J.; Soldatov, A.; Pushkar, Y. *J. Am. Chem. Soc.* **2011**, *133*, 15786−15794.
(46) van Lenthe, E.; Ehlers, A.; Baerends, E. J. *J. Chem. Phys.* **1999**, *110*, 8943−8953.
(47) Wang, F.; Ziegler, T.; van Lenthe, E.; van Gisbergen, S.; Baerends, E. J. *J. Chem. Phys.* **2005**, *122*, 204103.
(48) Wang, F.; Ziegler, T. *J. Chem. Phys.* **2005**, *123*, 154102.
(49) Vlček, A., Jr.; Záliš, S. *J. Phys. Chem. A* **2005**, *109*, 2991−2992.
(50) Záliš, S.; Ben Amor, N.; Daniel, C. *Inorg. Chem.* **2004**, *43*, 7978−7985.
(51) Rehr, J.; Albers, R. *Rev. Mod. Phys.* **2000**, *72*, 621−654.
(52) Joly, Y. *Phys. Rev. B* **2001**, *63*, 125120.
(53) DeBeer George, S.; Petrenko, T.; Neese, F. *Inorg. Chim. Acta* **2008**, *361*, 965−972.
(54) Záliš, S.; Farrell, I. R.; Vlček, A., Jr. *J. Am. Chem. Soc.* **2003**, *125*, 4580−4592.
(55) Záliš, S.; Busby, M.; Kotrba, T.; Matousek, P.; Towrie, M.; Vlček, A., Jr. *Inorg. Chem.* **2004**, *43*, 1723−1734.
(56) Vlček, A., Jr. *Coord. Chem. Rev.* **2002**, *230*, 225−242.
(57) Farrell, I. R.; van Slageren, J.; Záliš, S.; Vlček, A., Jr. *Inorg. Chim. Acta* **2001**, *315*, 44−52.
(58) Sato, S.; Sekine, A.; Ohashi, Y.; Ishitani, O.; Blanco-Rodríguez, A. M.; Vlček, A., Jr.; Unno, T.; Koike, K. *Inorg. Chem.* **2007**, *46*, 3531−3540.
(59) Sato, S.; Morimoto, T.; Ishitani, O. *Inorg. Chem.* **2007**, *46*, 9051−9053.
(60) Sato, S.; Matubara, Y.; Koike, K.; Falkenström, M.; Katayama, T.; Y., I.; Miyasaka, H.; Taniguchi, S.; Chosrowjan, H.; Mataga, N.;

Fukazawa, N.; Koshihara, S.; Onda, K.; Ishitani, O. *Chem.—Eur. J.* **2012**, *18*, 15722−15734.
(61) Vlček, A., Jr. *Coord. Chem. Rev.* **1998**, *177*, 219−256.
(62) Goumans, T. P. M.; Ehlers, A. W.; van Hemert, M. C.; Rosa, A.; Baerends, E. J.; Lammertsma, K. *J. Am. Chem. Soc.* **2003**, *125*, 3558−3567.

dx.doi.org/10.1021/ic3025843 | *Inorg. Chem.* 2013, 52, 5775−5785